

Equation of state and stability of the helium-hydrogen mixture at cryogenic temperature

Y. Safa^a and D. Pfneniger

Geneva Observatory, University of Geneva, 1290 Sauverny, Switzerland

Received 11 April 2008 / Received in final form 15 October 2008

Published online 4 December 2008 – © EDP Sciences, Società Italiana di Fisica, Springer-Verlag 2008

Abstract. The equation of state and the stability of the helium-molecular hydrogen mixture at cryogenic temperature up to moderate pressure are studied by means of current molecular physics methods and statistical mechanics perturbation theory. The phase separation, segregation and hetero-coordination are investigated by calculating the Gibbs energy depending on the mixture composition, pressure and temperature. Low temperature quantum effects are incorporated via cumulant approximations of the Wigner-Kirkwood expansion. The interaction between He and H₂ is determined by Double Yukawa potentials. The equation of state is derived from the hard sphere system by using the scaled particle theory. The behavior of the mixture over a wide range of pressure is explored with the excess Gibbs energy of mixing and the concentration fluctuations in the long wavelength limit. The theory is compared to cryogenic data and Monte-Carlo calculation predictions. Contrary to previous similar works, the present theory retrieves the main features of the mixture below 50 K, such as the critical point and the condensation-freezing curve, and is found to be usable well below 50 K. However, the method does not distinguish the liquid from the solid phase. The binary mixture is found to be unstable against species separation at low temperature and low pressure corresponding to very cold interstellar medium conditions, essentially because H₂ alone condenses at very low pressure and temperature, contrary to helium.

PACS. 64.10.+h General theory of equations of state and phase equilibria – 64.75.Gh Phase separation and segregation in model systems (hard spheres, Lennard-Jones, etc.) – 64.75.Ef Mixing

1 Introduction

Studying the mixing behavior of helium (⁴He) and molecular hydrogen (¹H₂) forming a binary system over a wide range of conditions is extremely important for astrophysical purposes in view of the ubiquity of this mixture in the Universe. As by-product, such as study is also of interest for industrial applications that need to extend the conditions accessible on Earth. The present work is a contribution to understand the stability of this important cosmic mixture in cryogenic conditions well below 100 K and for a pressure range going from 0 to a few kbar, therefore including in particular conditions found in the cold interstellar gas.

This work was motivated by the necessity to predict the behaviour of this mixture in conditions that are not easily observable yet, but that might be reached in cold molecular clouds far from excitation sources, such as those in outer galactic disks. Almost all earlier similar studies about the equation of state of He and H₂ have been focused on high temperature and high pressure conditions suited for planetary and stellar interiors (e.g., [1]).

The mutual solubility of a binary mixture with respect to the conditions of composition, temperature, pressure

and density is also of interest for non-astrophysical applications. For example, in metallurgy a fine dispersion of a phase during a melting process results in a significant improvement of the mechanical properties of materials as well as in the production of electrically and thermally well-conducting devices.

Generally, there are two distinct classes of mixtures according to their deviations from Raoult's law (i.e., the additive rule of mixing): a positive deviation corresponds to a segregating system, and a negative deviation corresponds to a short-ranged ordered alloy. The extreme deviations from Raoult's law may lead to either phase separation or compound formation in the binary system. In this work we examine such a deviation as it reflects the energetic and structure of constituting atoms. We use the excess Gibbs energy of mixing G_M^{xs} to evaluate the degree of segregation and the degree of miscibility of the binary mixture.

For metallurgic applications the present work may be helpful since, to our knowledge, very little studies have been carried out for the treatment of liquid alloys exhibiting segregation (like atoms tend to be as nearest neighbors) see Singh and Sommer [2].

The idea of representing a liquid by a system of hard spheres was originally proposed by Van Der Waals [3]; his

^a e-mail: yasser.safa@unige.ch

classical equation of state, which accounts qualitatively for the prediction of condensation and the existence of a liquid-vapour critical point was derived using essentially such a simple representation. In the case of a He–H₂ mixture a complication arises from the slight non-sphericity of H₂. In order to overcome this difficulty, following Ali et al. [4], we make use of the shape factor for the treatment of the model as a hard convex body derived from the hard spheres system. The application of such a tool, which is based on the scaling theory as proposed by Largo and Solana [5], is an advanced method for dealing with the nonsphericity of the constituents.

Until recently, most equations of state (EOS) have resulted from mathematical approximations of experimental data without a more fundamental theoretical basis. The strong point of the method adopted here is that the relation between pressure, temperature, density and concentration of components is derived from the sole knowledge of the intermolecular potentials. To describe the intermolecular repulsive and attractive interaction, we use the double Yukawa potential (DY) which provides an accurate analytical expression for the Helmholtz free energy.

When dealing with light species such as He and H₂ at low temperature, we need to take into account quantum mechanical effects. Both He and H₂ have 2 protons and 2 electrons: at first sight He appears just somewhat heavier than H₂. However the quantum rules and shapes related with the electronic orbitals change completely the macroscopic properties at low temperature. Below a few K, H₂ can condense even at very low pressure, while He remains fluid at normal pressure down to 0 K.

Ali et al. and others have used the Wigner-Kirkwood expansion (see [4]) to take into account to first order quantum effects of such a system. But after having checked and compared with experimental thermodynamical properties, we found that the Wigner-Kirkwood expansion diverges at temperatures below 50 K even if we extend the quantum correction to second order. To be able to reach at least the critical point of H₂ at 33 K, we searched in the literature for other methods and found the approach of Royer [6] adapted to our need. Quantum contributions are described via a renormalized Wigner-Kirkwood cumulant expansion around 0 K, which is well adapted for our objective to describe the mixture also well below the critical temperature, down to about the cosmic radiation background temperature of 2.73 K.

The paper is organized as follows: In this Section we have introduced the motivations for undertaking this work as a contribution in the study of the interstellar medium. In Section 2, we present the hypotheses on which our model is based, and we mention the related investigations that we are aware of already handled by other authors. In Section 3, we describe the intermolecular potential and the justification of the Double Yukawa potential to describe repulsive and attractive effects at the molecule level. The aim of Section 4 is to introduce the formulation of the Gibbs and Helmholtz energy via an analytical description based on the intermolecular potential and the diameter of hard spheres. Section 5 deals with the equation of state,

derived from the different contributions of the Helmholtz energy. In Section 6, we treat the phase stability of the mixture through the Gibbs energy. In Section 7, we introduce the major results of this study and some related discussion. Finally, the principal conclusions and perspectives corresponding to this work are summarized in Section 8.

2 Preliminary considerations

In this section we present the basic hypotheses for our study. We mention several related investigations handled by previous authors, in order to put this study in the context of other related researches.

Our model is based on the following hypotheses:

- The inter-molecular potential model used to describe the pairwise interaction of constituent species is the spherically symmetric pair potential containing a short range repulsion and a long range attraction components.
- The model of hard convex body is used to represent the geometry of the species in the mixture, it is derived from the hard sphere system based on the scaled particle theory SPT see [7]. A system of hard spheres represents the simplest realistic prototype for modeling the vapor-fluid phase separation in such a mixture.
- The mixture is considered as a pure neutral molecular phase, since we have a region of temperature T well below 1000 K and pressure P below 1 Mbar. In such conditions, molecular dissociation and ionization by pressure are not expected to occur. For details on the ionized plasma of the helium-hydrogen mixture at high pressure, see [8]. At low temperature and moderately low pressure, the transition from a molecular phase to an atomic phase ($\text{H}_2 \rightleftharpoons 2 \text{H}$) is not expected, further the presence of He stabilizes the molecules in the mixture as shown in [9]. In interstellar conditions neutrality is not always granted due to the frequent presence of ionizing and dissociating radiations allowing the coexistence of H and H₂. However, in “dense” molecular clouds ($n > 10^3 \text{ cm}^{-3}$, $3 < T < 50 \text{ K}$, still much less dense than the best industrial vacuum) almost all H is converted into H₂, so the He–H₂ mixture is the relevant one there.
- For P below 1 Mbar, the molecular-metallic transition is not reached. This will have an influence on the mixing conditions, especially since He is more soluble in H₂ than in metallic H as predicted by Stevenson and Salpeter [10]. Results about the solubility of He in metallic H are given by Stevenson [11], the properties of metallic H are studied under high dynamic pressures by Nellis [12] and the details on molecular-metallic transition of H are exposed by Chabrier [13].
- The effects of minor isotopic and trace species and ions in astrophysical conditions (D, Li, CO, H₂O, CH₄, NH₃, ...) are not included in model construction.
- The gravitational separation of phases is not included in our model. This hypothesis is justified by assuming the gravitational field negligible, or by considering a sufficiently small region at constant pressure.

Barotropic phenomena have been described in the H_2 -He system in the investigations of Street [14–16]. This system belongs to an unusual class of binary mixtures in which the more volatile component (He) has the higher molecular weight, and at high pressure may be more dense than the second component, even though the former may be a gas and the latter a solid or liquid in the pure state. As pressure passes through a corresponding value, the liquid phase rises up and floats on the top of the gas phase. By considering a region around the barotropic pressure, the coexisting phases have the same densities and the gravitational phase separation doesn't occur, at least for a limited time.

- Taking into account the condition of low temperature $T < 50$ K that we are interested in, the ortho-para composition of H_2 is considered here to be fully para- H_2 . This point might be improved in future works, because the ortho-para equilibrium can be well parametrized as a function of temperature.

3 Double Yukawa for the He– H_2 system

The estimation of the intermolecular potential energy inevitably involves assumptions concerning the nature of attraction and repulsion between molecules. Intermolecular interaction is resulting from both short-ranged repulsion u_{ij}^{HS} and long-ranged attraction (or “traction”) u_{ij}^{t}

$$u_{ij}(r) = u_{ij}^{\text{HS}}(r) + u_{ij}^{\text{t}}(r), \quad (1)$$

while the long-ranged attraction is treated as a perturbation and the short-ranged repulsion acts as an unperturbed reference (usually approximated by a repulsive hard sphere).

The Lennard-Jones potential is undoubtedly the most widely used intermolecular potential for molecular simulation. It is a simple continuous potential that provides an adequate description of intermolecular interactions for many applications at low pressure. But the inverse-power repulsion in LJ potential is inconsistent with quantum mechanical calculations and experimental data, which show that the intermolecular repulsion has an exponential character. For this purpose the exponential-6 (α -exp-6) potential is a reasonable choice instead of the LJ potential [17].

An anomalous property of the α -exp-6 potential, however, is that at a small distance r_c in the region of high temperature ($T > 2000$ K), the potential reaches a maximum value and in the limit $r \rightarrow 0$, it diverges to $-\infty$ [18]. As suggested in [4,19] the double Yukawa potential u^{DY} may be considered as advantageous since it can fit many other forms of empirical potentials, and, in addition, the related integral equation of the Helmholtz free energy and compressibility factor can be solved analytically:

$$u_{ij}^{\text{DY}} = \epsilon_{ij} A_{ij} \frac{\sigma_{ij}^0}{r} \left[e^{\lambda_{ij}(1-r/\sigma_{ij}^0)} - e^{\nu_{ij}(1-r/\sigma_{ij}^0)} \right], \quad (2)$$

where ϵ_{ij} represents the potential depth and σ_{ij}^0 the position at which the potential is zero (see Fig. 1).

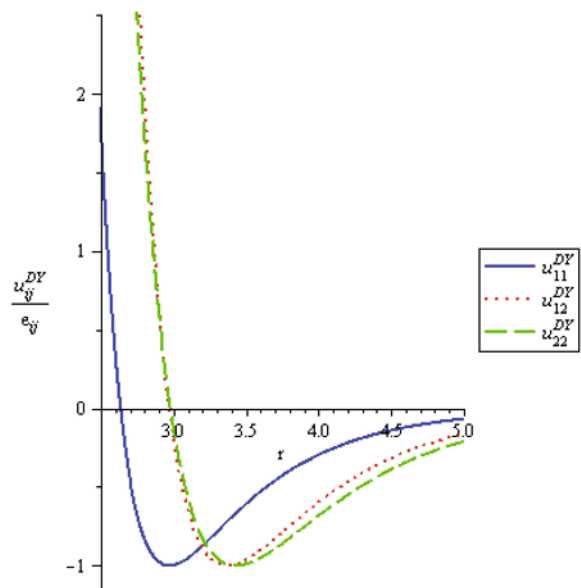


Fig. 1. The double Yukawa potential for the 3 possible pair interactions in the He– H_2 mixture.

Table 1. DY potential parameters in the He– H_2 mixture.

| | He–He | H_2 – H_2 | He– H_2 |
|-----------------------|--------|-----------------------------|------------------|
| i, j | 1.1 | 2.2 | 1.2 |
| σ_{ij}^0 (Å) | 2.634 | 2.978 | 2.970 |
| ϵ_{ij}/k (K) | 10.57 | 36.40 | 15.50 |
| A_{ij} | 2.548 | 3.179 | 2.801 |
| λ_{ij} | 12.204 | 9.083 | 10.954 |
| ν_{ij} | 3.336 | 3.211 | 3.386 |

The terms A_{ij} , λ_{ij} and ν_{ij} control the magnitude of the repulsive and attractive contributions of the double Yukawa potential. The parameters (Tab. 1) are suitably chosen to provide a close fit to the exp-6 potential proposed in [17].

The controlling parameters (Tab. 1) are slightly non-additive, i.e., $A_{12} \approx (A_{11} + A_{22})/2$, $\lambda_{12} \approx (\lambda_{11} + \lambda_{22})/2$ and $\nu_{12} \approx (\nu_{11} + \nu_{22})/2$. In contrast, the potential depth ϵ_{ij} is strongly nonadditive

$$\epsilon_{12} = \alpha \sqrt{\epsilon_{11}\epsilon_{22}}, \quad (3)$$

where the nonadditive parameter α quantifies the relative strength of the unlike pairwise interaction. In our case ($\alpha \approx 0.79 < 1$) and the molecules are not energetically alike. We are, hence, concerned with a non-athermal mixture (i.e., we don't have energetically alike species $\epsilon_{11} = \epsilon_{22} = \epsilon_{12}$). In such a situation the contribution to the free energy is predicted to be arising from both enthalpic and entropic effects. According to [4] the smaller value of α (compared to 1) should drive the mixtures towards demixing.

4 Gibbs energy of mixing

Considerable efforts have been spent in the recent years to propose a fundamental physical theory describing the

reasons responsible for phase separation in a binary mixture.

Thermodynamically, the Gibbs energy of mixing G_M which depends on the enthalpy H_M and the entropy S_M , is of great interest. In fact, by evaluating its deviation from the Gibbs value of an ideal mixture G_{id} , the energetic term G_M provides the crucial informations on the thermodynamic stability of the mixture. Obviously the process could be complicated by the respective enthalpic or entropic contributions to segregation (for details, see [2]). The term G_M is expressed as

$$G_M = G - \sum_i c_i G_i^0, \quad (4)$$

where c_i are the mole fractions, G is the Gibbs free energy of the mixture and $G_i^0 = G(c_i \rightarrow 1)$ is the free energy of the pure constituent species i . The variable G relates the pressure P to the Helmholtz free energy F

$$\frac{G}{NkT} = \frac{F}{NkT} + \frac{P}{nkT}, \quad (5)$$

where T , n^1 , N and k are respectively the temperature, the number density, the total number of molecules, and Boltzmann's constant.

4.1 Hard convex body free energy

The total Helmholtz energy F for a mixture of N molecules is obtained from

$$\frac{F}{N} = F^{id} + F^{HB} + F^t + F^Q, \quad (6)$$

where F^{id} is the Helmholtz energy per molecule arising from the ideal gas mixture. It is defined with

$$\beta F^{id} = \frac{3}{2} \ln \left(\frac{h^2}{2\pi kT m_{11}^{c_1} m_{22}^{c_2}} \right) + \ln n + \sum_i c_i \ln c_i - 1, \quad (7)$$

where h is the Planck's constant, m_{ii} are the atomic masses and β is the inverse temperature $\beta = 1/kT$.

The Helmholtz free energy F^{HB} for the hard convex body is given by

$$\beta F^{HB} = a_{\text{mix}} \beta (F^{\text{HS}} + F^{\text{nonadd}}), \quad (8)$$

where the coefficient a_{mix} is the nonsphericity parameter and will be presented in details bellow, the term F^{HS} is the Helmholtz energy of hard sphere, and F^{nonadd} is the contribution arising from the nonadditivity of the hard sphere diameter.

The expression of F^{HS} reads (see e.g., [19])

$$\beta F^{\text{HS}} = \frac{\eta_3 (f_1 + (2 - \eta_3)f_2)}{1 - \eta_3} + \frac{\eta_3 f_3}{(1 - \eta_3)^2} + (f_3 + 2f_2 - 1) \ln(1 - \eta_3), \quad (9)$$

¹ Note that sometimes ρ is used instead of n in the chemical-physics literature, which leads to confusion with the elsewhere widely adopted meaning of ρ as the mass density.

where the parameters in equation (9) are related to the hard spheres diameters σ_{ij} by

$$f_1 = \frac{3y_1y_2}{y_0y_3}, \quad (10)$$

$$f_2 = \frac{y_1y_2}{y_3^3} (y_4z_1 + y_0z_2), \quad (11)$$

$$f_3 = \frac{y_2^3}{y_0y_3^3}, \quad (12)$$

$$y_i = \frac{\eta_i}{n}, \quad (13)$$

$$\eta_i = \frac{\pi}{6} n (c_1 \sigma_{11}^i + c_2 \sigma_{22}^i), \quad (14)$$

$$z_1 = 2c_1c_2\sigma_{11}\sigma_{22} \frac{\sigma_{11} - \sigma_{22}}{\sigma_{11} + \sigma_{22}}, \quad (15)$$

$$z_2 = c_1c_2\sigma_{11}\sigma_{22}^3 (\sigma_{11}^2 - \sigma_{22}^2). \quad (16)$$

The distances σ_{ij} are calculated via the integration of the correlation function

$$\sigma_{ij} = \int_0^{\sigma_{ij}^0} (1 - e^{-\beta u_{ij}(r)}) dr. \quad (17)$$

According to [20], equation (17) may be derived from the minimization of the free energy difference between the reference fluid (a purely short range repulsive model) and the effective hard sphere model (including the long range attraction). The use of equation (17) makes σ_{ij} temperature dependent and enables us to investigate the effect of temperature on G_M and consequently the impact of temperature and pressure on the mixing conditions of binary mixture (heterocoordination, segregation or phases separation). Subsequently, by taking into account the enthalpy-entropy relation ($S_M = -\partial G_M / \partial T$), the T dependence of G_M paves the way to illustrate the entropic contributions of binary mixture with respect to T and P .

4.2 Non-additive free energy

The positive nonadditivity of hard sphere diameters ($\sigma_{12} > (\sigma_{11} + \sigma_{22})/2$) is predicted to cause an instability of binary mixture as shown in many works (see for example [21–24]). Although in the conclusion of the latter the negative nonadditivity of hard sphere diameters ($\sigma_{12} < (\sigma_{11} + \sigma_{22})/2$) is considered to not exhibit a fluid-fluid demixing, however in [25] a demixing transition in binary hard sphere mixture is possible for a slightly negative nonadditivity. The drawback of the major approaches is that σ_{ij} remains independent of T and hence its applicability is limited.

On a more realistic basis the T dependence of σ_{ij} introduced via equation (17) is desirable to study the non-additivity effect and the phase diagram of the mixture, as shown by [19,26].

The contribution F^{nonadd} is obtained by means of the first order perturbation correction [27]

$$\beta F^{\text{nonadd}} = -4\pi n c_1 c_2 \bar{\sigma}_{12}^2 \Delta \sigma_{12} g_{12}^{\text{HS}}(\sigma_{12}), \quad (18)$$

with

$$\bar{\sigma}_{12} = \frac{\sigma_{11} + \sigma_{22}}{2} \quad \text{and} \quad \Delta\sigma_{12} = \bar{\sigma}_{12} - \sigma_{12}. \quad (19)$$

Here the term $g_{12}^{\text{HS}}(\sigma_{12})$ refers to the radial distribution function $g_{12}(r)$ for a hard sphere model at the contact point $r = \sigma_{12}$ (conventionally the term $g_{ij}^{\text{HS}}(r)$ is noted RDF and it measures the extent to which the positions of particle center deviate from those of uncorrelated ideal gas).

The contact values of RDF $g_{ij}^{\text{HS}}(\sigma_{ij})$ consists of the improved versions given in [28,29], denoted by $g_{ij}^{\text{BMCSL}}(\sigma_{ij})$, and the correction term, $g_{ij}^{\text{BS}}(\sigma_{ij})$, suggested by [30] to improve the contact value of the pair correlation function

$$g_{ij}^{\text{HS}}(\sigma_{ij}) = g_{ij}^{\text{BMCSL}}(\sigma_{ij}) + g_{ij}^{\text{BS}}(\sigma_{ij}), \quad (20)$$

the values of the terms $g_{ij}^{\text{BMCSL}}(\sigma_{ij})$ are introduced by Tang and Benjamin [31] as

$$g_{ij}^{\text{BMCSL}}(\sigma_{ij}) = g_{ij}^{(0)}(\sigma_{ij}) + g_{ij}^{(1)}(\sigma_{ij}), \quad (21)$$

where $g_{ij}^{(0)}(\sigma_{ij})$ is the contact value of the Percus-Yevick radial distribution function (PY RDF)

$$g_{ij}^{(0)}(\sigma_{ij}) = \frac{1}{1 - \eta_3} + \frac{3\eta_2}{(1 - \eta_3)^2} \frac{\sigma_{ii}\sigma_{jj}}{\sigma_{ii} + \sigma_{jj}} \quad (22)$$

and $g_{ij}^{(1)}(\sigma_{ij})$ is the first-order RDF at contact point, given by

$$g_{ij}^{(1)}(\sigma_{ij}) = \frac{2\eta_2^2}{(1 - \eta_3)^3} \left(\frac{\sigma_{ii}\sigma_{jj}}{\sigma_{ii} + \sigma_{jj}} \right)^2. \quad (23)$$

The terms $g_{ij}^{\text{BS}}(\sigma_{ij})$ are given by

$$g_{ij}^{\text{BS}}(\sigma_{ij}) = \frac{1 - \delta_{ij}c_i}{2} \frac{\eta_1\eta_2}{(1 - \eta_3)^2} \frac{D(\sigma_{11} - \sigma_{22})}{\bar{\sigma}_{ij}} \frac{\sigma_{ii}\sigma_{jj}}{\left(\delta_{ij} + (1 - \delta_{ij}) \frac{\sigma_{22}}{\sigma_{11}} \right)}, \quad (24)$$

where δ_{ij} is the Kronecker Delta function, D the reduced collision parameter

$$D = \frac{\sigma_{11}\sigma_{22}}{2\bar{\sigma}_{12}}, \quad (25)$$

and

$$\bar{\sigma}_{ij} = \frac{\sigma_{ii} + \sigma_{jj}}{2}. \quad (26)$$

4.3 Shape factor

The coefficient a_{mix} in equation (8) is the nonsphericity parameter or the shape factor. It scales the excess compressibility factor of a hard sphere mixture to obtain that corresponding to the HCB (hard convex body) mixture. Following the works of Largo and Solana [5,32], we have

$$a_{\text{mix}} = \frac{1}{V_{\text{mix}}} \sum_{ij} c_i c_j V_{ij}^{\text{ef}} a_{ij}^{\text{ef}}, \quad (27)$$

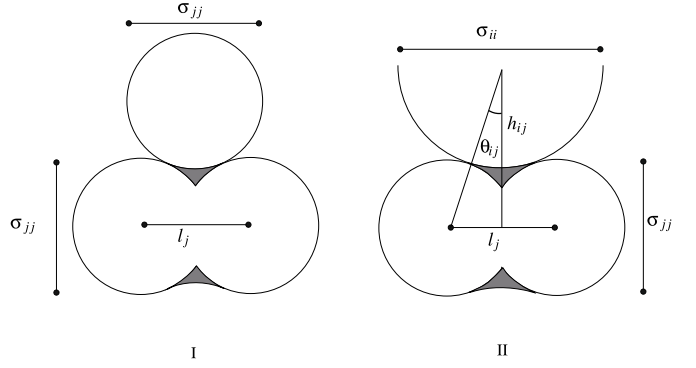


Fig. 2. The shaded area represents the difference between effective and real molecular volume of a hard dumbbell: (I) as “seen” by a sphere of the same diameter as the one of the dumbbell spheres, (II) as “seen” by a bigger sphere.

with

$$V_{\text{mix}} = \sum_{ij} c_i c_j V_{ij}^{\text{ef}}, \quad (28)$$

where V_{ij}^{ef} is the effective volume of the molecule i as “seen” by a molecule of species j

$$V_{ij}^{\text{ef}} = \frac{\pi}{6} \sigma_{ij}^3 \bar{V}_{ij}, \quad (29)$$

and a_{ij}^{ef} is the effective nonsphericity parameter a_{ij}^{ef} defined in the form

$$a_{ij}^{\text{ef}} = \frac{1}{3\pi} \frac{(V_{ij}^{\text{ef}})' (V_{ij}^{\text{ef}})''}{V_{ij}^{\text{ef}}}, \quad (30)$$

where $'$ and $''$ denote the first and second derivatives with respect to σ_{ij}

$$(V_{ij}^{\text{ef}})' = \left(\frac{\partial V_{ij}^{\text{ef}}}{\partial \sigma_{ii}} \right)_{\sigma_{jj}} + \left(\frac{\partial V_{ij}^{\text{ef}}}{\partial \sigma_{jj}} \right)_{\sigma_{ii}}, \quad (31)$$

$$(V_{ij}^{\text{ef}})'' = \left(\frac{\partial^2 V_{ij}^{\text{ef}}}{\partial \sigma_{ii}^2} \right)_{\sigma_{jj}} + 2 \frac{\partial^2 V_{ij}^{\text{ef}}}{\partial \sigma_{ii} \partial \sigma_{jj}} + \left(\frac{\partial^2 V_{ij}^{\text{ef}}}{\partial \sigma_{jj}^2} \right)_{\sigma_{ii}}, \quad (32)$$

and \bar{V}_{ij} is the average molecular volume, estimated as function of n_i , the number of elemental spheres of diameter σ_{ii} , and of the center to center distance l_i (see Fig. 2)

$$\bar{V}_{ij} = 1 + (n_i - 1) \left[\frac{3}{2} \left(1 + \frac{\sigma_{ij}^2}{\sigma_{ii}^2} \right) L_i - \frac{1}{2} L_i^3 - 3 \frac{h_{ij}}{\sigma_{ii}} \theta_{ij} \left(\frac{\sigma_{jj}^2}{\sigma_{ii}^2} \right) \right], \quad (33)$$

where

$$L_i = \frac{l_i}{\sigma_{ii}}, \quad (34)$$

$$h_{ij} = \frac{1}{2} \sqrt{(\sigma_{ii} + \sigma_{jj})^2 - l_i^2}, \quad (35)$$

$$\theta_{ij} = \arcsin \left(\frac{l_i}{\sigma_{ii} + \sigma_{jj}} \right). \quad (36)$$

While the He average molecular volume is equal to 1, the average H₂ molecular volume is about 1.3, this will have an important influence on the thermodynamic predictions, especially for mixtures of cosmic interest that contain about 90% of H₂ mole fraction

4.4 Attraction free energy

At high temperature and pressure, the stiffness and the range of the intermolecular repulsion play dominant roles. It is the case when the detonation velocity of condensed explosives are investigated [17], or in the Jupiter and Saturn's interiors ($5 \times 10^3 < T < 10^4$ K and $P \approx 200$ GPa.), where the long-ranged molecular attraction contribution becomes negligible. In contrast, at low temperature and pressure, for predicting properly the vapour-liquid transition both the repulsive and attractive effects must be included.

In equation (6), the term F^t is the first order perturbation contribution due to long-ranged attraction. Statistical mechanics provides an evaluation of F^t via the integral equation including the radial distribution functions $g_{ij}(r)$ and the potentials $u_{ij}^{\text{DY}}(r)$:

$$\beta F^t = \beta \frac{n}{2} \sum_{ij} c_i c_j \int_{\sigma_{ij}^0}^{\infty} u_{ij}^{\text{DY}}(r) g_{ij}^{\text{HS}}(r, \sigma_{ij}, n) 4\pi r^2 \bar{V}_{ij} dr. \quad (37)$$

Using the respective Laplace transforms of the functions $r g_{ij}^{\text{HS}}(r)$

$$G_{ij}(s) = \int_0^{\infty} r g_{ij}^{\text{HS}}(r) e^{-sr} dr, \quad \forall s \in \mathbb{R}. \quad (38)$$

Equation (37) can be brought to

$$\beta F^t = \frac{2\pi n}{kT} \sum_{ij} c_i c_j \epsilon_{ij} \sigma_{ij}^0 A_{ij} \bar{V}_{ij} \left(e^{\lambda_{ij}} G\left(\frac{\lambda_{ij}}{\sigma_{ij}^0}\right) - e^{\nu_{ij}} G\left(\frac{\nu_{ij}}{\sigma_{ij}^0}\right) \right) - \delta F^t, \quad (39)$$

where δF^t is the value of the integral on the interval $[\sigma_{ij}, \sigma_{ij}^0]$

$$\delta F^t = \beta \frac{n}{2} \sum_{ij} c_i c_j \int_{\sigma_{ij}}^{\sigma_{ij}^0} u_{ij}^{\text{DY}}(r) g_{ij}^{\text{HS}}(r) 4\pi r^2 \bar{V}_{ij} dr. \quad (40)$$

The subtraction of δF^t is important due to the fact that the interval $[\sigma_{ij}, \sigma_{ij}^0]$ is covered by equation (38) and does not belong to the attractive range $[\sigma_{ij}^0, \infty]$.

Regarding the intersection of the functions $u_{ij}^{\text{DY}}(r) g_{ij}^{\text{HS}}(r)$ and $u_{ij}^{\text{DY}}(r) g_{ij}^{\text{HS}}(\sigma_{ij})$ at $r = \sigma_{ij}$ and $r = \sigma_{ij}^0$ respectively, by considering the close variations of these functions in the interval $[\sigma_{ij}, \sigma_{ij}^0]$, we can approach the value of δF^t by numerical integration of the

expression

$$\delta F^t \approx \beta \frac{n}{2} \sum_{ij} c_i c_j \int_{\sigma_{ij}}^{\sigma_{ij}^0} u_{ij}^{\text{DY}}(r) g_{ij}^{\text{HS}}(\sigma_{ij}) 4\pi r^2 \bar{V}_{ij} dr. \quad (41)$$

The contact values of the radial distribution functions $g_{ij}^{\text{HS}}(\sigma_{ij})$ are found by equation (20–24).

The details of the analytical expressions of the functions $G_{ij}(s)$ are given in Tang and Benjamin [31].

4.5 Quantum free energy

The term F^Q in equation (6) corresponds to the first order quantum correction of the Wigner-Kirkwood expansion [33,34]

$$\beta F^Q = \frac{h^2 \beta^2 N_A n}{96\pi^2} \sum_{ij} \frac{c_i c_j}{m_{ij}} \times \int_{\sigma_{ij}}^{\infty} \nabla^2 u_{ij}^{\text{DY}}(r) g_{ij}^{\text{HS}}(r, \sigma_{ij}, n) 4\pi r^2 \bar{V}_{ij} dr. \quad (42)$$

Using equation (38) we can obtain F^Q in term of Laplace transforms

$$\beta F^Q = \frac{h^2 \beta^2 N_A n}{24\pi} \sum_{ij} \frac{c_i c_j \epsilon_{ij} A_{ij} \bar{V}_{ij}}{m_{ij} \sigma_{ij}^0} \times \left(\lambda_{ij}^2 e^{\lambda_{ij}} G\left(\frac{\lambda_{ij}}{\sigma_{ij}^0}\right) - \nu_{ij}^2 e^{\nu_{ij}} G\left(\frac{\nu_{ij}}{\sigma_{ij}^0}\right) \right). \quad (43)$$

After checks we find that the first order quantum correction exhibits a poor convergence for temperature $T < 50$ K. Although the second order correction of Wigner-Kirkwood expansion extends somewhat the convergence over colder systems, it is still by far insufficient at cryogenic temperatures, e.g., in the case of pure He with temperature T less than 40 K, [35].

We recall that one may suggest the application of quantum correction to the hard sphere diameter σ_{ij} , [36], via the relation

$$\sigma_{\text{cor}} = \sigma + \frac{\lambda}{8}, \quad (44)$$

where λ is the de Broglie wavelength $\lambda = \sqrt{\beta \hbar^2 / 2m}$.

This correction is usable at high temperature, but insufficient for obtaining reasonable description of quantum effects at cryogenic temperature $T < 50$ K.

4.6 Renormalized Wigner-Kirkwood expansion

To describe the He–H₂ mixture at such low temperature, we have used the renormalized Wigner-Kirkwood cumulant expansion [6]. This is a reasonable choice since it is usable down to zero temperature.

In order to obtain a renormalized cumulant approximation of the Wigner-Kirkwood (WK) expansion, following Royer [6] we make use, for simplicity, the following

one-dimensional treatment which could be extended to the multi-dimensional case.

We denote by $n_V(X)$ the quantum Boltzmann density at the space coordinate X

$$n_V(X) = \langle X | e^{-\beta H_V} | X \rangle, \quad (45)$$

where H_V is the Hamiltonian of a particle of mass m moving with momentum p in the potential V

$$H_V = \frac{p^2}{2m} + V. \quad (46)$$

The classical approximation of Boltzmann density reads

$$n_{V,cl}(X) = \frac{1}{2\sqrt{\pi}\lambda} e^{-\beta V(X)}. \quad (47)$$

Let us consider $W(x)$ the quadratic potential approximating $V(x)$ around the point X ,

$$W(x) = V(X) + V'(X)(x - X) + \frac{1}{2}V''(X)(x - X)^2. \quad (48)$$

We expand $\ln n_V(X)$, instead of $n_V(X)$, in powers of the potential difference $v = V - W$. By Taylor expanding $v(x)$ about X in the cumulant expansion, we obtain an expansion which is a resummation over power of $V''(X)$ of the WK expansion of $\ln n_V(X)$. Provided $V''(X) > 0$, this expansion remains a useful approximation even when $T \rightarrow 0$.

According to the standard formalism of statistical quantum mechanics, in a domain Λ of a N -particle fluid, the partition functions Z_q and Z_{cl} corresponding to $n_V(X)$ and $n_{V,cl}(X)$ respectively, are given by

$$Z_q = \frac{1}{N!} \int_{\Lambda} n_V(X) dX \quad (49)$$

and

$$Z_{cl} = \frac{1}{N!} \int_{\Lambda} n_{V,cl}(X) dX. \quad (50)$$

With the free energy F_{qu} , defined by the relation

$$-\beta F_{qu} = \ln Z_{qu}. \quad (51)$$

We can readily obtain an estimation of the quantum Helmholtz energy correction F^Q as

$$F^Q = \left(\frac{\ln Z_q}{\ln Z_{cl}} - 1 \right) (F^{id} + a_{mix} (F^{HS} + F^{nonadd})). \quad (52)$$

The detail on the complicated expression of the cumulant expansion with respect to the choice of the local approximating potential $W(x)$ are given in [6]. We note that the ratio $\ln Z_q / \ln Z_{cl}$ should approach unity in the case of high temperature where the quantum free energy is neglected, while for $T = 100\text{K}$ the ratio $\ln Z_q / \ln Z_{cl}$ takes a value corresponding to the first order WK.

In our computational implementation we can choose to use either the renormalized cumulant expansion, or the first order WK, since the latter is simpler to calculate.

5 The equation of state

As mentioned by Jung et al. [37], at the boundary of a fluid-fluid phase change, we must obtain an equal value for the Gibbs free energies of different phases. Since a small error in the free energy expression can significantly shift the position of the phase boundary, we need then an accurate equation of state (EOS) for determining correctly the critical phase change curve and the critical point.

In the chemical picture, by dealing with a pure molecular system without dissociation the compression ratio tends to increase considerably because of internal degree of freedom of the molecules (rotations and vibrations) [38].

Let us introduce the subscripts: $b \in \{\text{HB}, \text{t}, \text{Q}, \text{id}, \text{nonadd}, \text{HS}\}$ which carry the same meaning as in equations (6) and (8). The compressibility factor Z^b is expressed via the thermodynamic relation

$$Z^b = n \frac{\partial}{\partial n} \left(\frac{F^b}{kT} \right). \quad (53)$$

It is easy to see that from equations (53) and (7) we have the behaviour of the ideal gas mixture

$$Z^{id} = n \frac{\partial}{\partial n} \left(\frac{F^{id}}{kT} \right) = 1. \quad (54)$$

With equation (53) and by taking into account equation (8), the compressibility factor Z^{HB} can be expressed as

$$\begin{aligned} Z^{\text{HB}} &= n \frac{\partial}{\partial n} \left(\frac{F^{\text{HB}}}{kT} \right) \\ &= a_{mix} \left(n \frac{\partial}{\partial n} (\beta F^{\text{HS}}) + n \frac{\partial}{\partial n} (\beta F^{\text{nonadd}}) \right) \\ &= a_{mix} (Z^{\text{HS}} + Z^{\text{nonadd}}), \end{aligned} \quad (55)$$

where

$$\begin{aligned} Z^{\text{HS}} &= n \frac{\partial}{\partial n} \left(\frac{F^{\text{HS}}}{kT} \right) \\ &= \frac{1}{1 - \eta_3} + \frac{3\eta_1\eta_2}{\eta_0(1 - \eta_3)^2} + \frac{\eta_2^3(3 - \eta_3)}{\eta_0(1 - \eta_3)^3} \\ &\quad + \frac{\eta_1\eta_2(\eta_4 z_1 + \eta_0 z_2)}{(1 - \eta_3)^2}. \end{aligned} \quad (56)$$

Similarly, the correction term of compressibility factor Z^{nonadd} which arises from the non-additivity of hard spheres is expressed as

$$\begin{aligned} Z^{\text{nonadd}} &= n \frac{\partial}{\partial n} \left(\frac{F^{\text{nonadd}}}{kT} \right) \\ &= -4\pi n c_1 c_2 \bar{\sigma}_{12}^2 \Delta\sigma_{12} \left(g_{12}^{\text{HS}}(\sigma_{12}) \right. \\ &\quad \left. + n \left(\frac{\partial g_{12}^{\text{HS}}(\sigma_{12})}{\partial n} \right)_c \right). \end{aligned} \quad (57)$$

By applying the partial derivative with respect to n given in (53) in the relation (39), we obtain the compressibility factor corresponding to the attractive effects Z^t

$$\begin{aligned} Z^t = & \frac{2\pi n}{kT} \sum_{ij} c_i c_j \epsilon_{ij} \sigma_{ij}^0 A_{ij} \bar{V}_{ij} \left(e^{\lambda_{ij}} \left(G\left(\frac{\lambda_{ij}}{\sigma_{ij}^0}\right) \right. \right. \\ & + n \frac{\partial}{\partial n} G\left(\frac{\lambda_{ij}}{\sigma_{ij}^0}\right) \left. \left. - e^{\nu_{ij}} \left(G\left(\frac{\nu_{ij}}{\sigma_{ij}^0}\right) \right. \right. \right. \\ & \left. \left. \left. + n \frac{\partial}{\partial n} G\left(\frac{\nu_{ij}}{\sigma_{ij}^0}\right) \right) \right) \right) - \delta Z^t, \end{aligned} \quad (58)$$

where δZ^t corresponds to the integral in the interval $[\sigma_{ij}, \sigma_{ij}^0]$, which is evaluated by numerical integration of the expression

$$\begin{aligned} \delta Z^t \approx & \beta \frac{n}{2} \sum_{ij} c_i c_j \left(g_{ij}^{\text{HS}}(\sigma_{ij}) + n \frac{\partial g_{ij}^{\text{HS}}(\sigma_{ij})}{\partial n} \right) \\ & \times \int_{\sigma_{ij}}^{\sigma_{ij}^0} u_{ij}^{\text{DY}}(r) 4\pi r^2 \bar{V}_{ij} dr. \end{aligned} \quad (59)$$

The terms $g_{ij}^{\text{HS}}(\sigma_{ij})$ and the derivatives $\partial g_{ij}^{\text{HS}}(\sigma_{ij})/\partial n$ can be readily obtained from equations (20–24).

The expression of the compressibility factor Z^Q corresponding to the first order quantum correction of Wigner-Kirkwood expansion is obtained from equation (43)

$$\begin{aligned} Z^Q = & \frac{h^2 \beta^2 N_A n}{24\pi} \sum_{ij} \frac{c_i c_j \epsilon_{ij} A_{ij} \bar{V}_{ij}}{m_{ij}^2 \sigma_{ij}^0} \left(\lambda_{ij}^2 e^{\lambda_{ij}} \left(G\left(\frac{\lambda_{ij}}{\sigma_{ij}^0}\right) \right. \right. \\ & + n \frac{\partial}{\partial n} G\left(\frac{\lambda_{ij}}{\sigma_{ij}^0}\right) \left. \left. - \nu_{ij}^2 e^{\nu_{ij}} \left(G\left(\frac{\nu_{ij}}{\sigma_{ij}^0}\right) \right. \right. \right. \\ & \left. \left. \left. + n \frac{\partial}{\partial n} G\left(\frac{\nu_{ij}}{\sigma_{ij}^0}\right) \right) \right) \right). \end{aligned} \quad (60)$$

The pressure P in equation (5) can be directly obtained by summing the respective compressibility factors

$$P = nkT (1 + Z^{\text{HB}} + Z^t + Z^Q). \quad (61)$$

The resulting pressure should be treated by a Maxwell construction when density $n(P, T)$ at a fixed T becomes multi-valued. We describe in Appendix A an iterative method to carry out this construction.

6 Phase stability

There are different ways to investigate the conditions of phase stability of a mixture [39]. The first one is through the calculation of the Gibbs energy as in equation (5). The condition for the stability of the mixture is

$$\left(\frac{\partial^2 G}{\partial c^2} \right)_{T,P} > 0. \quad (62)$$

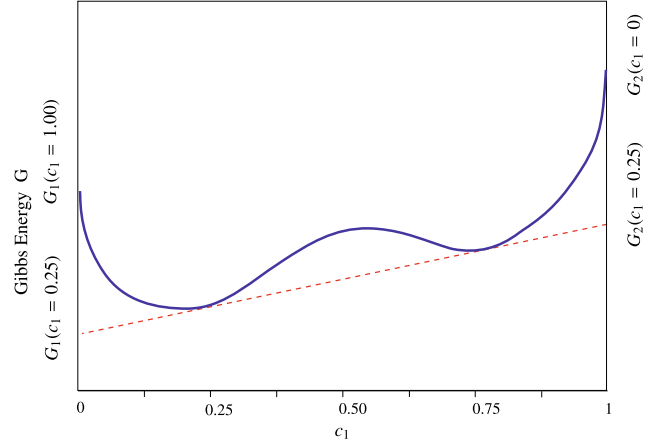


Fig. 3. Common tangent construction for a binary mixture model. The coexisting compositions $c_1 = 0.25$ and $c_1 = 0.75$ lie on the same tangent, thus having the same free energy for the two components.

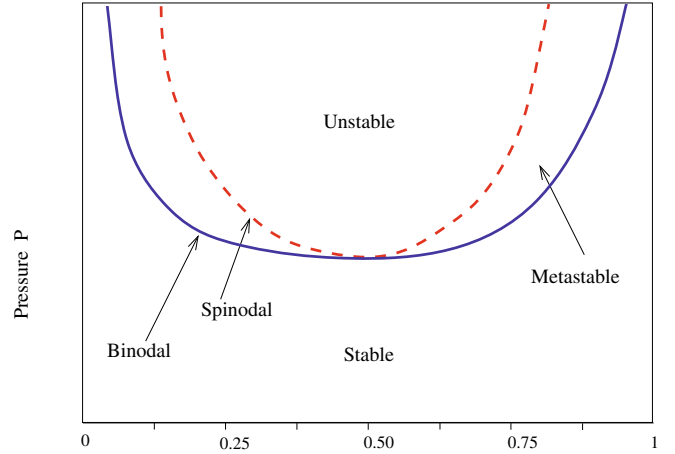


Fig. 4. Phase diagram of a binary mixture model.

When the free energy curve is not entirely convex, i.e., it has also concave part with points associated with a negative curvature ($(\partial^2 G/\partial c^2)_{T,P} < 0$) the mixture is no longer stable as a single phase. In such a case it is possible to find two points on the curve that share the same tangent and consequently the free Gibbs energy of both components at these compositions are the same (see Fig. 3). In other words, these compositions can coexist in equilibrium. By mean of this graphical method known as the method of double tangent or common tangent construction, we can find the locus of the coexisting points in (P, c) plan at constant temperature known as the binodal curve.

The point of instability corresponds to

$$\left(\frac{\partial^2 G}{\partial c^2} \right)_{T,P} = 0, \quad (63)$$

and the locus of these points in (P, c) plan at constant temperature, defines the spinodal curve which is the border of the stability of the mixture (see Fig. 4).

Let us assume that the principal process which leads to phase instability is a trend towards the aggregation

between particles of the same species. An other and efficient method to control the mixing behavior at atomic level is to compute the concentration-concentration fluctuation

$$S_{cc}(0) = NkT \left(\frac{\partial^2 G}{\partial c^2} \right)_{T,P}^{-1}. \quad (64)$$

This quantity, compared to the ideal values $S_{cc}^{\text{id}} = c_1 c_2$, provides valuable insight on the degree of order and the thermodynamic stability of the mixture. In atomic picture, at given composition c_1 , the positive deviation from ideal $S_{cc}(0) > S_{cc}^{\text{id}}$ is an indication of a tendency to segregation (like atoms tend to pair as nearest neighbors). In contrast the negative deviation from ideal $S_{cc}(0) < S_{cc}^{\text{id}}$ corresponds to heterocoordinations (unlike atoms tend to pair as nearest neighbors). The extreme deviations $S_{cc}(0) \rightarrow \infty$ and $S_{cc}(0) \rightarrow 0$ are respectively corresponding to phase separations and complete heterocoordinations (compound formation).

7 Results

The results are presented in two steps: first, we compare Monte Carlo simulations (MC) and Molecular Dynamic computations (MD) with our He–H₂ mixture model described above, and programmed in a FORTRAN-90 code called AstroPE. Second, we describe the thermodynamic behavior of the He–H₂ mixture, including quantum corrections, under cryogenic conditions or potentially interesting cases for the cold interstellar medium.

7.1 Comparisons with pure He and H₂ simulations and data

By taking the required input from Table 1 we have obtained the theoretical values of pressure for different values of temperature T and He concentration c_1 . In Table 2 we introduce a comparison between our computed values of the pressure and the results of Monte Carlo (MC) simulation presented by Ree [17]. In this work, the He–H₂ mixture is considered as a van der Waals one fluid model and the intermolecular potential is the exp-6 potential.

We observe a reasonable agreement between our results and those corresponding to the MC simulations, which are usually considered as sufficiently accurate. The quantum effect is not included in the above comparison. Nevertheless, in our calculation, for a temperature $T = 100$ K, the quantum corrections raise P by about 15%, which corresponds to the first order correction of the Wigner-Kirkwood expansion as estimated in [17]. For higher temperature the obtained values of P are not affected significantly by the quantum contribution.

On the other hand, we have compared our results in the case of pure He with those resulting from the work of Koei et al. [40]. In this latter work the Buckingham potential is used to perform molecular dynamics (MD) simulations of He for studying the phase transitions and the melting points.

In Figures 5–8 we present the variation of the pressure with respect to the density for some given values of the

Table 2. Comparison of the pressure P resulting from our AstroPE FORTRAN-90 code with the pressure corresponding to Ree [17] MC simulations. The corresponding values of the reduced density n^* are listed. Quantum effects are not included.

| T (K) | c_1 | V (cm ³ /mol) | n^* | P MC (GPa) | P AstroPE (GPa) |
|------------|-------|-------------------------------|---------|-----------------|----------------------|
| 50 | 0.50 | 20.0 | 0.03011 | 0.0473 | 0.0441 |
| 100 | 0.50 | 14.0 | 0.04301 | 0.3380 | 0.3550 |
| 300 | 0.25 | 10.0 | 0.06022 | 2.3090 | 2.6987 |
| 300 | 0.50 | 10.0 | 0.06022 | 1.8560 | 2.1389 |
| 300 | 0.75 | 10.0 | 0.06022 | 1.4240 | 1.5371 |
| 1000 | 0.25 | 9.0 | 0.06691 | 5.2550 | 5.2978 |
| 1000 | 0.50 | 9.0 | 0.06691 | 4.5100 | 4.7319 |
| 1000 | 0.75 | 9.0 | 0.06691 | 3.7150 | 3.7955 |
| 4000 | 0.50 | 8.0 | 0.07528 | 12.4300 | 12.2877 |
| 4000 | 0.50 | 7.0 | 0.08603 | 16.3300 | 16.0603 |

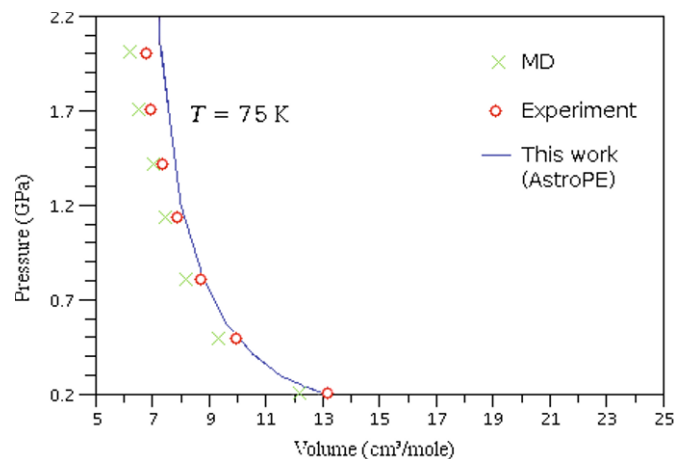


Fig. 5. The pressure of pure He compared to the values of MD simulations and experimental results at temperature $T = 75$ K.

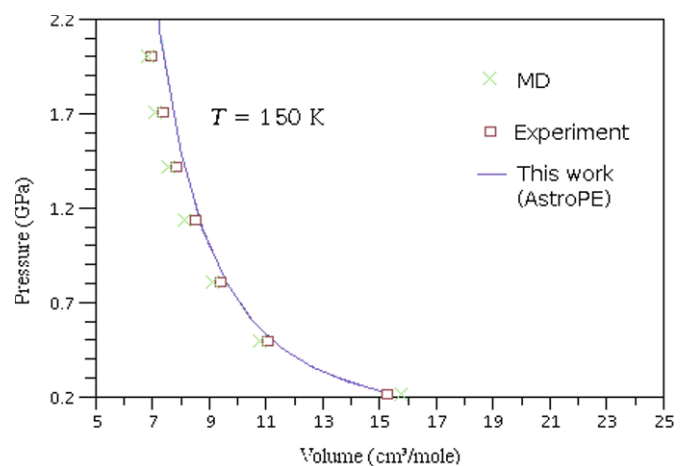


Fig. 6. The pressure of pure He compared to the values of MD simulations and the experimental results at temperature $T = 150$ K.

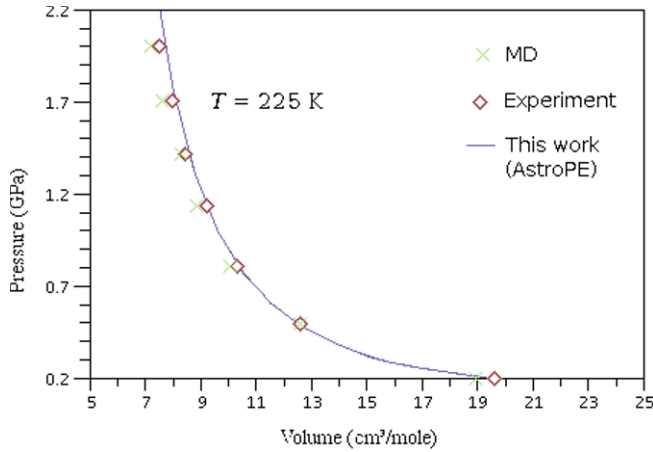


Fig. 7. The pressure of pure He compared to the values of MD simulations and the experimental results at temperature $T = 225$ K

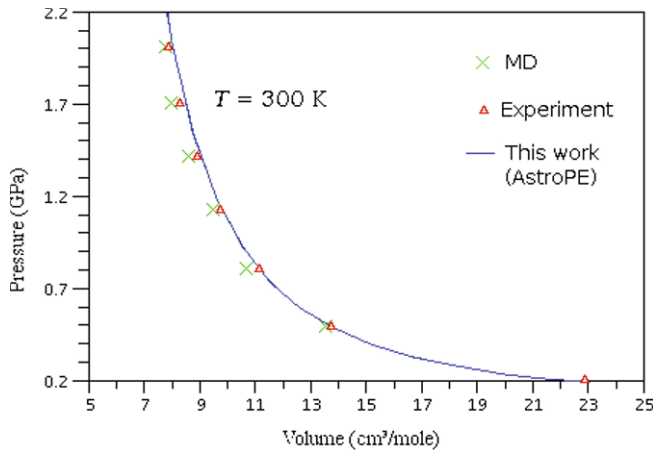


Fig. 8. The pressure of pure He compared to the values of MD simulations and the experimental results at temperature $T = 300$ K.

temperature. The lines represent the variation resulting from our computations. The cross symbols correspond to the MD results, whereas the other symbols are related to the experimental data as reported in [40].

The match of our results with the experimental data is almost perfect especially for the region of low pressure. The MD results exhibit a good agreement with the reference data in the case of high pressure since the model in [40] is expected to be valid at high pressures, but not for very low pressures, where quantum effects dominate the solid state properties.

In Figure 9 we compare densities on the 0.85 MPa isobar in the temperature range 18 to 300 K, coming from experimental data, other theoretical predictions, and from our program AstroPE. The experimental data comes from [41], the Path Integral simulation (PI) comes from Wang et al. [42]. The phase transition on the 0.85 MPa isobar at about 30 K is well visible. Clearly the overall behaviour is reproduced, but the absolute value of density in the condensed phase may differ by a up a factor 9%.

A simple but stringent test for using our model at cryogenic temperature is to check the positions of the

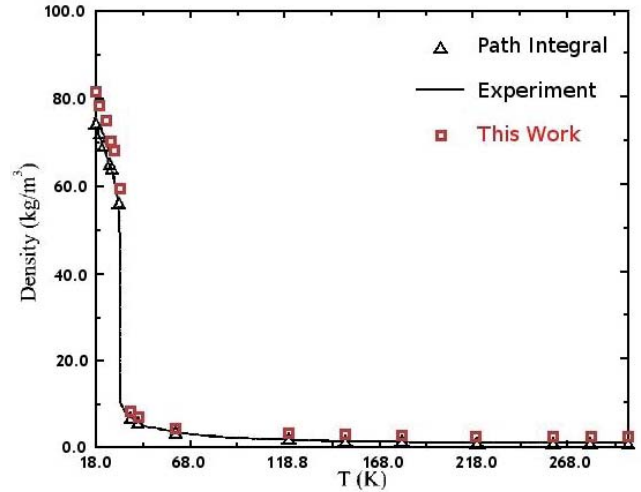


Fig. 9. Fluid densities on isobar $P = 0.85$ MPa as a function of temperature. The curve is the experimental data from [41] and the symbols are from path integral simulations [42] and from this work.

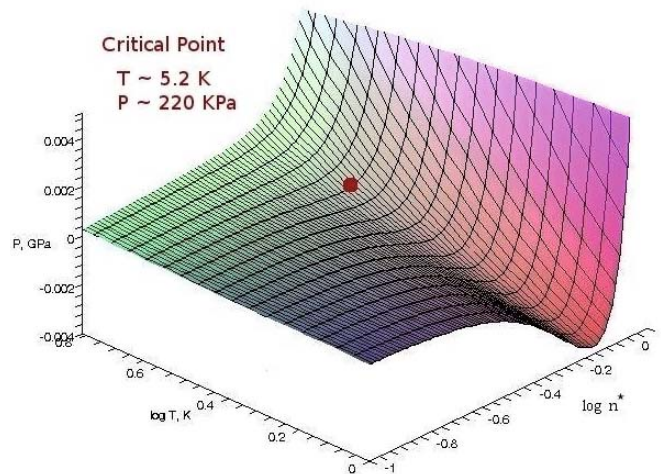


Fig. 10. The pressure of the pure He without Maxwell construction. The reported critical point is located at $P_c \approx 220$ kPa and $T_c \approx 5.2$ K.

respective critical point of He and H_2 , that are determined by searching a point where $\partial P(T, n)/\partial n = 0$ and $\partial^2 P(T, n)/\partial n^2 = 0$ at constant T for $P(T, n)$ uncorrected by the Maxwell construction.

For He we find the critical point at $P_c \approx 220$ kPa and $T_c \approx 5.2$ K, and for H_2 at $P_c \approx 1300$ kPa and $T_c \approx 32$ K. Numerical noise in the saddle point evaluation prevents us to give more digits. Industrial cryogenic gas reference [43] gives $P_c = 227.5$ kPa and $T_c = 5.2$ K for He, and $P_c \approx 1298$ kPa and $T_c \approx 32.976$ K for para- H_2 , and $P_c \approx 1298$ kPa and $T_c \approx 33.24$ K for normal- H_2 .

In Figures 10–13 we show the equation of state for pure He and H_2 with and without the corresponding Maxwell construction. The algorithm to determine the Maxwell construction is sketched in Appendix A.

Overall the agreements between our results and those corresponding to MC simulation and MD simulation and

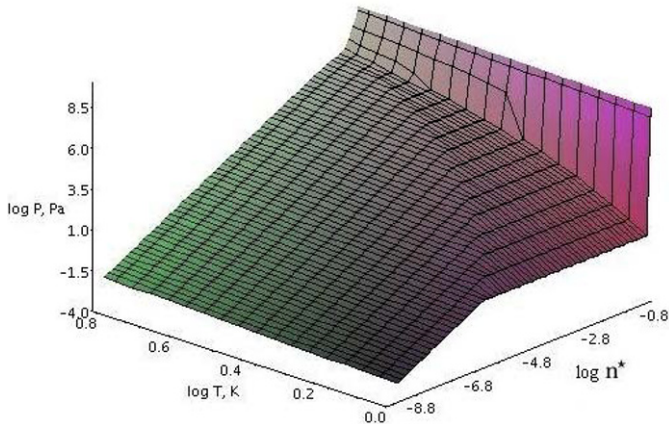


Fig. 11. The pressure of the pure He with Maxwell construction.

Critical Point:

$T \sim 32 \text{ K}$
 $P \sim 1300 \text{ kPa}$

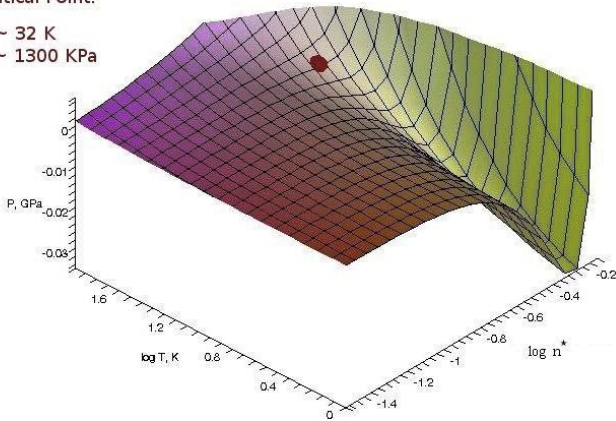


Fig. 12. The pressure of pure H_2 without Maxwell construction. The reported critical point is located at $P_c \approx 1300 \text{ kPa}$ and $T_c \approx 32 \text{ K}$.

experimental data show that our equation of state is usable already for the pure substances over a wide range of temperature and pressure, including the cryogenic and low pressure regimes that we are interested in.

7.2 Thermodynamic results on the He– H_2 mixture

Here we present the calculated thermodynamic properties of the He– H_2 mixture under cryogenic conditions and low pressure, suited for some interstellar medium conditions, where the He concentration amounts to about 11%. Figures 14 and 15 show surface plots of the compressibility factors corresponding to the Hard Body repulsive and attractive effects respectively. The results are reported for 2 ranges of reduced density's values: $10^{-44} < n^* < 10^{-4}$ (left side) and $10^{-4} < n^* < 10^{-1}$ (right side). The temperature range is $1 \leq T \leq 80 \text{ K}$. Logarithmic scales are used when possible. In Figure 15 we plotted $\text{arcsinh}(Z^t)$ to provide good representation at large negative and positive values of the attraction compressibility factor.

Similarly, in Figure 16 we present the compressibility factor Z^Q . Clearly quantum effects are important at high density and low temperature.

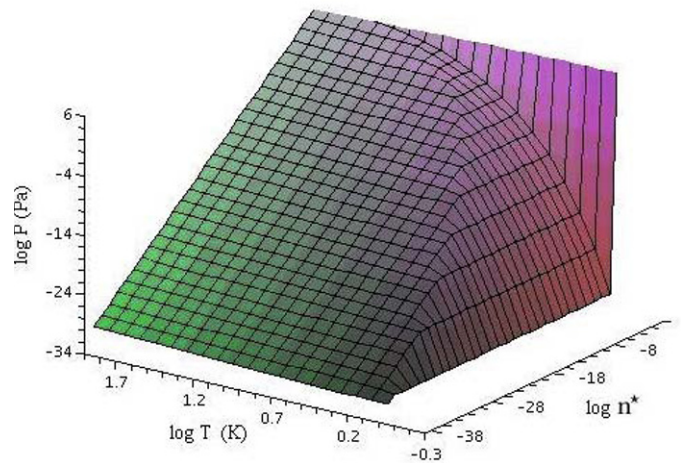


Fig. 13. The Pressure of the pure H_2 with Maxwell construction.

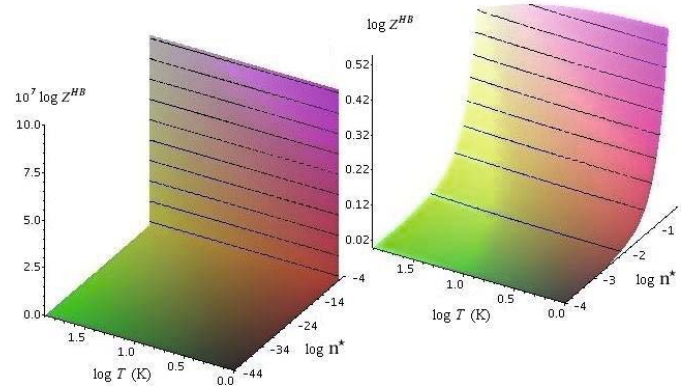


Fig. 14. The compressibility factor corresponding to Hard Body repulsive effects in the mixture of 11% Helium. The values are reported in the range of low density (left) and in the range of high density (right).

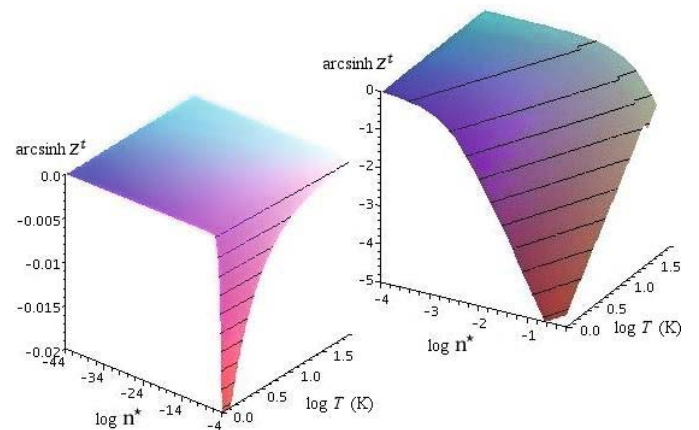


Fig. 15. The compressibility factor corresponding to the traction effects in the mixture of 11% Helium. The values are reported in the range of low density (left) and in the range of high density (right).

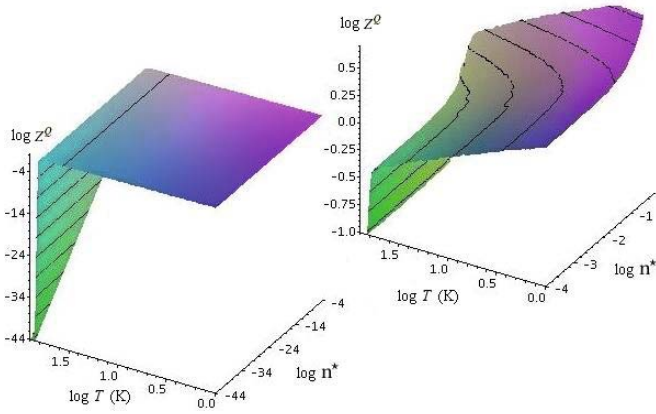


Fig. 16. The compressibility factor corresponding to the quantum effects in the mixture of 11% Helium. The values are reported in the range of low density (left) and in the range of high density (right).

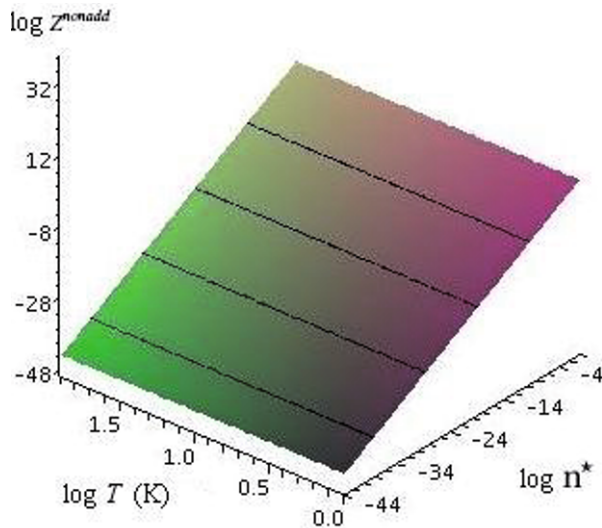


Fig. 17. The compressibility factor corresponding to the non-additivity a mixture of 11% Helium.

The compressibility factor Z^{nonadd} and the packing factor η_3 are shown in Figures 17 and 18 respectively. We observe a similar behavior of Z^{nonadd} and η_3 since the nonadditivity depends on the radial distribution function at the contact point $g_{ij}(\sigma_{ij})$ which relates to the values of the packing factor as given in (22) and (23).

The pressure is plotted as function of the temperature and the reduced density in Figure 19.

The phase boundaries of the mixture are given in Figure 20 including also the transition lines of pure constituents: the H_2 gas-condensed phase boundary and the He gas-liquid phase boundary.

An important point to take into account is that the pressure-induced solidification of a He- H_2 mixture is quite different from that of pure constituent. In the latter the melting pressure is only temperature dependent, but in the mixture the added degree of freedom allows fluid and solid to coexist over wide ranges of pressure at fixed temperature and vice versa [16].

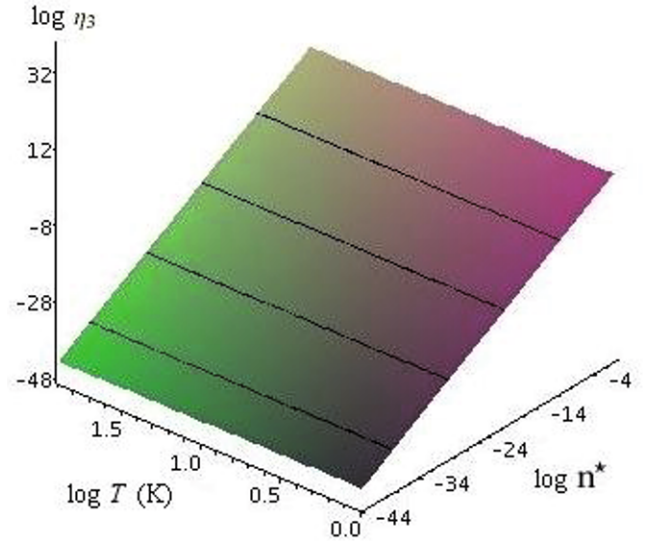


Fig. 18. The packing factor η_3 for the mixture of 11% Helium.

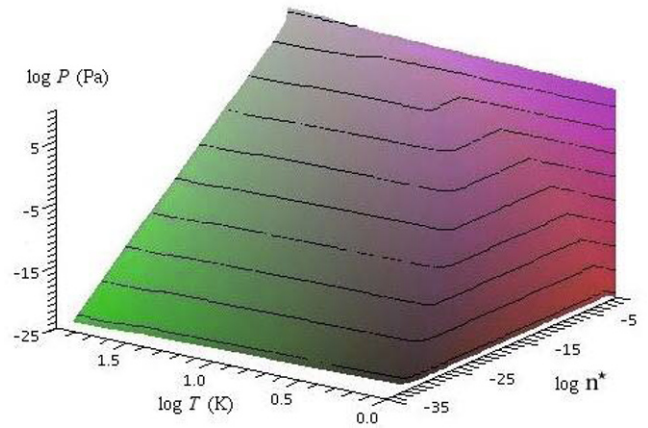


Fig. 19. The pressure P for the mixture of 11% Helium. Maxwell construction is carried out.

In Figure 20 we observe the effect of adding 11% He in H_2 . The transition line between the gas and condensed phase is shifted into the region of higher pressure.

At low temperature and low pressure suitable for some regions of the interstellar medium at $T \leq 10$ K, we computed the excess Gibbs energy for the mixture of 11% He. Figure 21 shows the value of the reduced excess Gibbs energy are introduced without applying the common tangent construction. It is easy to see that in the pressure-temperature domain ($\log P, \log T$) is globally separated in two regions corresponding to the deviations from the ideal mixing behavior. Clearly, sufficiently cold dilute He- H_2 gas will separate below a critical pressure, even at the very low pressures expected in “dense” molecular clouds if the temperature drops much below 5 K.

The use of the concentration-concentration fluctuation tool enables us to investigate efficiently the stability of the mixture at the atomic level. We compute the reduced concentration fluctuations $S_{cc}^*(0) = S_{cc}(0)/S^{\text{id}}$. The stable and unstable regions are thus reported in a surface plot in Figure 22. As mentioned in Section 6, this quantity

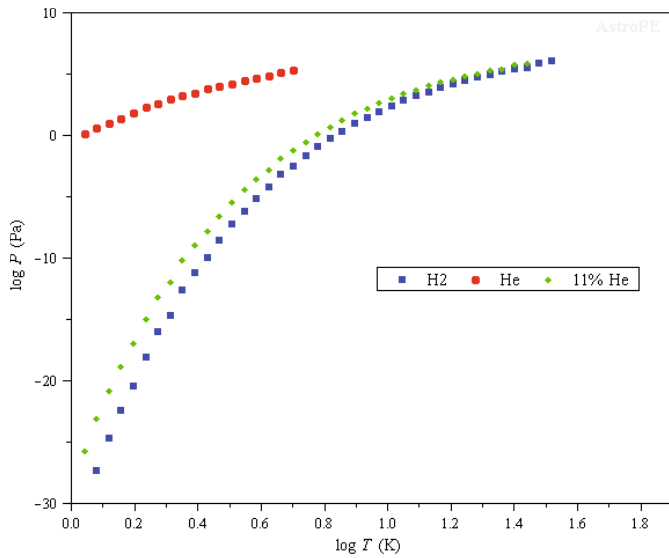


Fig. 20. Phase boundaries: the gas-solid phase boundary for pure Hydrogen, the gas-liquid phase boundary for pure Helium and the gas-condensed phase boundary for Helium-Hydrogen mixture.

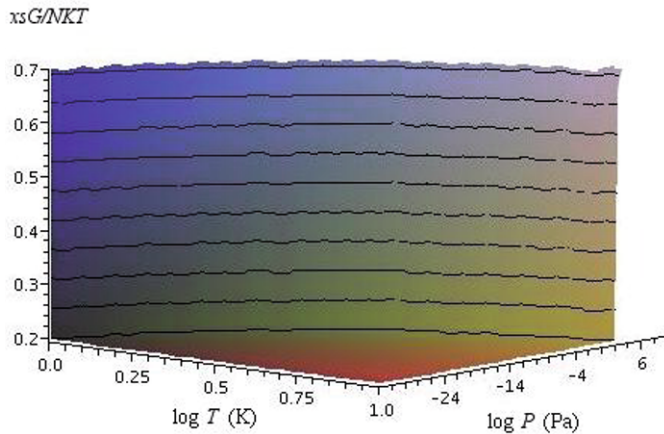


Fig. 21. Excess Gibbs energy for the mixture of 11% Helium.

provides the degree of order and the thermodynamic stability of the mixture in the atomic picture. The extreme values $S_{cc}^*(0) \gg 1$ observed in Figure 22 correspond to phase separation in the unstable region. On the other hand, the values $S_{cc}^*(0) \rightarrow 0$ are an indication of heterocoordination in the stable region. By choosing an orthogonal view of the above figure, the value of the reduced concentration fluctuations are also shown in two dimensions in Figure 23. By reproducing the computation of $S_{cc}^*(0)$ without including the quantum effects, we obtain the corresponding stability graph shown in Figure 24. Clearly when comparing Figures 23 and 24 we see that the quantum effect is important for the delimitation of the stability region.

We observe the correlation between the results in Figures 20, 21 and 23 in the delimitation of the temperature-pressure conditions for which the mixture of 11% He exhibited a phase separation between gas region of stable mixture and condensed phase region of unstable mixture.

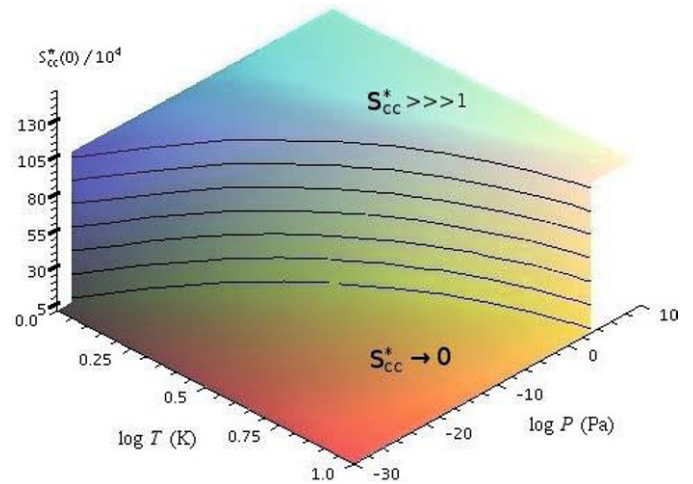


Fig. 22. The reduced concentration-concentration fluctuation for a mixture of 11% He computed using the common tangent construction.

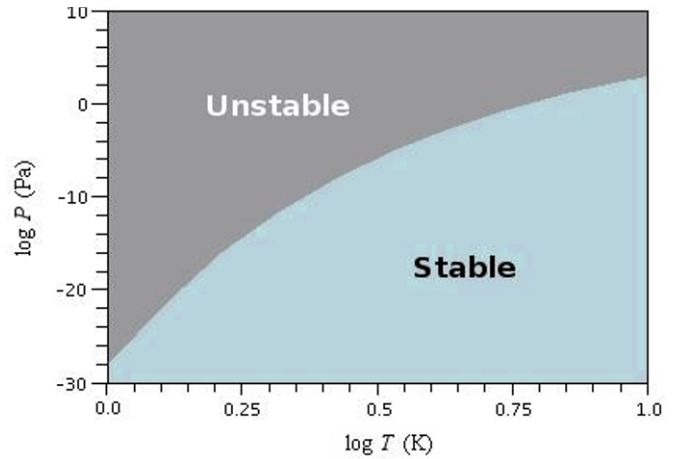


Fig. 23. The regions of stable and unstable mixture corresponding to the reduced concentration-concentration fluctuation for a mixture of 11% He.

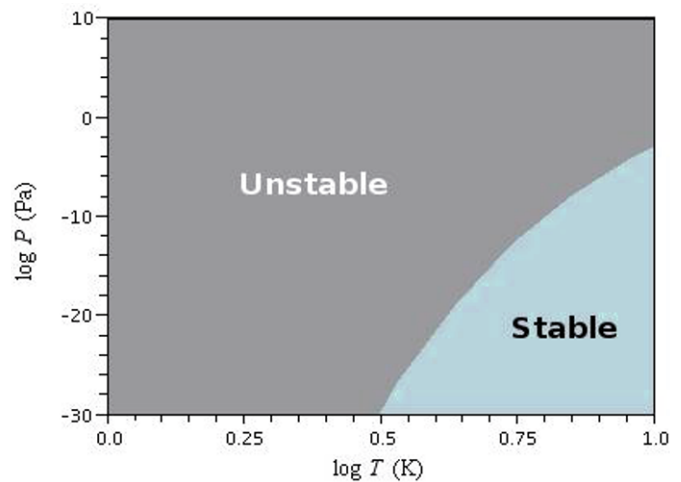


Fig. 24. The regions of stable and unstable mixture without quantum effect corresponding to the reduced concentration-concentration fluctuation for a mixture of 11% He.

8 Conclusion

In a region of low temperature such as in the interstellar medium, a direct observation of the phase separation of He–H₂ mixture is not possible because the emitted radiations is low and partly hidden by the universal cosmic radiation at 2.726 K. The strong quantum effect related to both the lightest and most abundant elements in the Universe makes the thermodynamic behavior of the mixture more difficult to model. In this study we have established a working tool to investigate the stability of the He–H₂ mixture at a temperature below 100 K. The equation of state is analytically derived from the knowledge of the pair spherical potentials to which quantum corrections are superposed. The results are in satisfactory correspondence with the experimental data as well as with MD and MC simulations for being useful in applications that do not require very high precision. As in a metallurgical approach the region of mixing and demixing are predicted by means of the concentration-concentration fluctuations tools. The He–H₂ mixture shows a phase separation in the region of very low temperature and low to high pressure. The results are suited for a study with hydrodynamics of the evolution of the cold and “dense” interstellar medium clouds or denser cold objects.

We thank S.M. Osman for interesting e-mail exchanges. This work is supported by Swiss National Science Foundation; Grant No. 200020-107766.

Appendix A: Maxwell construction

Below are given in pseudo-code the steps used to achieve the Maxwell construction: for a given isothermal $P(V)$ curve associated with a phase transition, such as shown in Figure 25,

we want to find the value \tilde{P} and the volumes V_l and V_r such that the integral $\int_{V_l}^{V_r} (P - \tilde{P}) dV = 0$. This condition is applied to verify the mechanical energy conservation, it may be formulated in term of the number density n by applying the variable change:

$$V = \frac{N}{n} \quad \Rightarrow \quad dV = -\frac{N}{n^2} dn.$$

The problem is then to find the three numbers n_l , n_r and \tilde{P} such that:

$$\int_{n_l}^{n_r} \frac{P - \tilde{P}}{n^2} dn = 0,$$

and $P(n_l) = P(n_r) = \tilde{P}$. Isolating \tilde{P} we have:

$$\tilde{P}(n_l, n_r) = \frac{n_l n_r}{n_r - n_l} \int_{n_l}^{n_r} \frac{P}{n^2} dn.$$

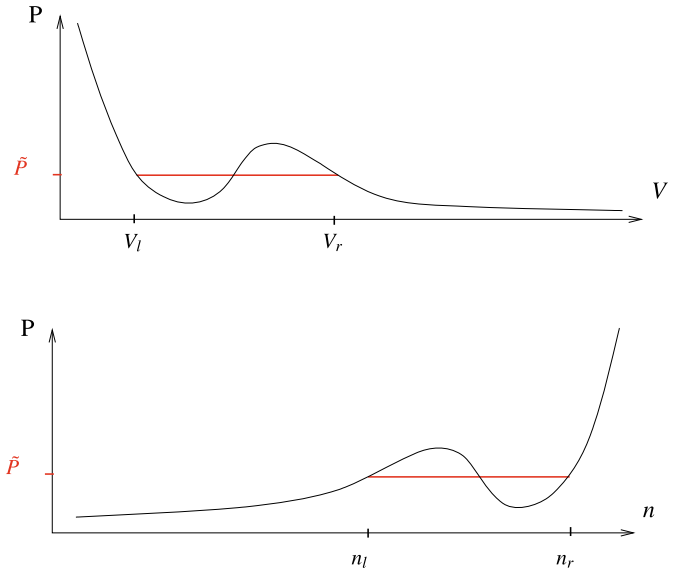


Fig. 25. Maxwell construction.

Clearly \tilde{P} depends on n_l and n_r , so we have in fact a problem with two equations and two unknowns: $P(n_l) = P(n_r) = \tilde{P}(n_l, n_r)$.

Let us apply the following discretization of the interval $[n_l, n_r]$:

$$[n_l, n_r] = \bigcup_{i=1}^{M-1} [n_i, n_{i+1}],$$

where $n_1 = n_l$, $n_M = n_r$. We define the i^{th} incrementation of the density number as:

$$\Delta n_i = n_{i+1} - n_i,$$

and we introduce the i^{th} mean value $P_i = (P(n_i) + P(n_{i+1}))/2$, the term \tilde{P} which depends on (n_l, n_r) can then be approximated by a numerical quadrature:

$$\tilde{P}(n_l, n_r) \simeq \frac{n_l n_r}{n_r - n_l} \sum_{i=1}^{M-1} \frac{P_i}{n_i^2} \Delta n_i. \quad (65)$$

Algorithm

- Starting step: (see Fig. 26)
 - Find the local extremum points: (P_l^0, n_l^0) and (P_r^0, n_r^0)
 - Set: $(n_l, n_r) = (n_l^0, n_r^0)$ (initialization of interval corresponding to the density jump)
 - Set: $(P_l, P_r) = (P_l^0, P_r^0)$
 - Compute: $\tilde{P} = \tilde{P}(n_l, n_r)$ (see Eq. (65))
- Iterative correction step: (see Fig. 27)
 - do while $(|P_l - P_r| > \epsilon)$
 - if $(\tilde{P} < P(n_l - \Delta n_l))$ then

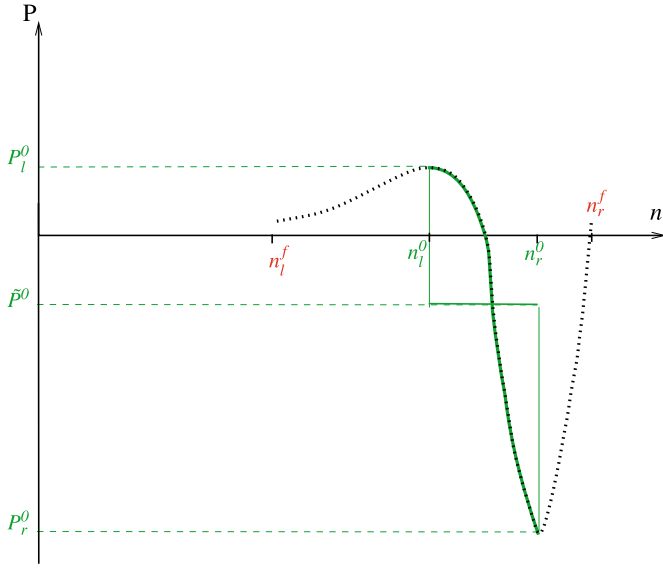


Fig. 26. Initialization step (0): $P_r^0 < \tilde{P}^0 < P_l^0$.

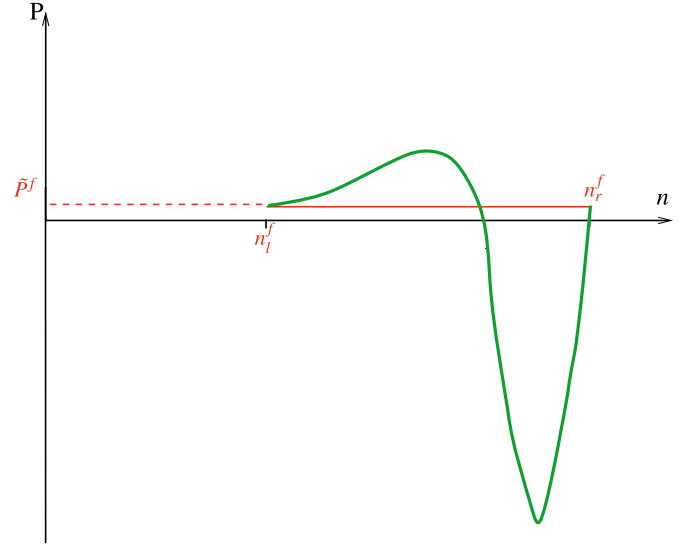


Fig. 28. Convergence at iterative step (f): $P_r^f = \tilde{P}^f = P_l^f$.

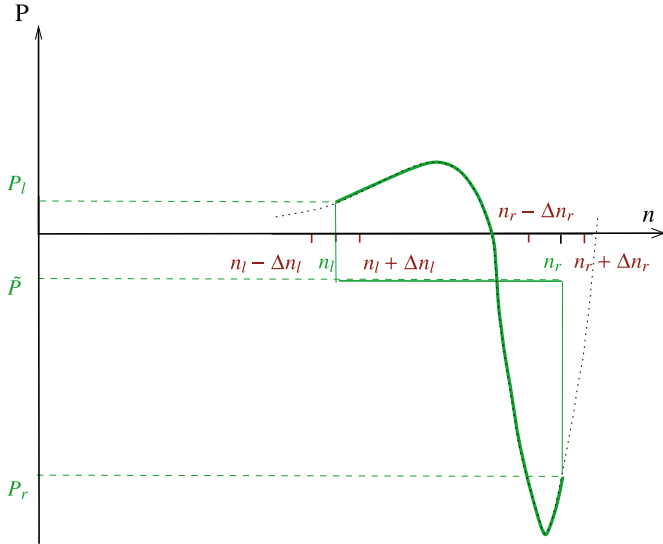


Fig. 27. An example of iterative step where: $P_r < \tilde{P} < P_l$.

```

- Set:  $n_l = n_l - \Delta n_l$  (the interval is enlarged at the
  left side)
- Compute:  $\tilde{P} = \tilde{P}(n_l, n_r)$  (see Eq. (65))
- Set:  $P_l = P(n_l)$ 
endif
if ( $\tilde{P} > P(n_r + \Delta n_r)$ ) then
- Set:  $n_r = n_r + \Delta n_r$  (the interval is enlarged at the
  right side)
- Compute:  $\tilde{P} = \tilde{P}(n_l, n_r)$ 
- Set:  $P_r = P(n_r)$ 
endif
enddo
P-Maxwell =  $\tilde{P}$ 
    
```

References

1. T. Guillot, *Ann. Rev. Earth Plan. Sc.* **33**, 493 (2005)
2. R.N. Singh, F. Sommer, *Rep. Prog. Phys.* **60**, 57 (1997)
3. J.D. Van Der Waals, *The Equation of State for Gases and Liquids* (Nobel Lecture, 1910)
4. I. Ali, S.M. Osman, N. Sulaiman, R.N. Singh, *Mol. Phys.* **101**, 3239 (2003)
5. J. Largo, J.R. Solana *Phys. Rev. E* **58**, 2251 (1998)
6. A. Royer, *Phys. Rev. A* **32**, 1729 (1985)
7. D.W. Siderius, D.S. Corti *Ind. Eng. Chem. Res.* **45**, 5489 (2006)
8. B. Militzer, *Proceedings to 5th Conferences on Crystals and Quantum Crystal in Worklaw*, Poland, 2004
9. J. Vorberger, I. Tamblyn, B. Militzer S.A. Bonev, *Phys. Rev. B* **75**, 024206 (2007)
10. D.J. Stevenson, E.E. Salpeter, *The Astrophys. J. Supl. Ser.* **35**, 221 (1977)
11. D.J. Stevenson, *J. Phys. F: Metal Phys.* **9**, 791 (1979)
12. W.J. Nellis, *J. Phys.: Cond. Matter* **14**, 11045 (2002)
13. G. Chabrier et al., *Astrophys. J.* **391**, 817 (1992)
14. W.B. Streett, in *Planetary Atmospheres, Proceedings of the Int. Astron. Union Symp.* **40**, 1971, pp. 363–370
15. W.B. Streett, *The Astrophys. J.* **186**, 1107 (1973)
16. W.B. Streett, *Icarus* **29**, 173 (1976)
17. F.H. Ree, *Mol. Phys.* **96**, 87 (1983)
18. I.A. Schouten, A. Kuijper, J.P.J. Michels, *Phys. Rev. B* **44**, 13 (1991)
19. I. Ali, S.M. Osman, N. Sulaiman, R.N. Singh, *Phys. Rev. E* **59**, 1028 (2004)
20. Y. Tang, W. Jianzhong, *J. Chem. Phys.* **119**, 7388 (2003)
21. F.H. Ree, *Proceedings of the joint AIRAPTS/APS Conferences* (Colorado Spring, CO, 1993)
22. F.A.-S. Basel, *Macromol. Theory Simul.* **9**, 772 (2000)
23. J.H. Nixon, M. Silbert, *Mol. Phys.* **52**, 207 (1984)
24. A.A. Louis, R. Finken, J.P. Hansen, *Phys. Rev. E* **61**, 1028 (2000)
25. A. Santos, M. Lopez de Haro, *Phys. Rev. E* **72**, 0110501 (2005) <http://arxiv.org/abs/cond-mat/0409718v2>

26. S.M. Osman, R.N. Singh, *Mol. Phys.* **96**, 87 (1999)
27. E.W. Grundke et al., *Mol. Phys.* **25**, 883 (1973)
28. T. Boublik, *J. Chem. Phys.* **53**, 471 (1970)
29. G.A. Mansoori et al., *J. Chem. Phys.* **54**, 1523 (1971)
30. C. Barrio, J.R. Solana, *J. Chem. Phys.* **113**, 180 (2000)
31. Y. Tang, C.-Y.L. Benjamin, *J. Chem. Phys.* **103**, 7463 (1995)
32. J. Largo, J.R. Solana *Mol. Phys.* **96**, 1367 (1999)
33. E.P. Wigner, *Phys. Rev.* **40**, 749 (1932)
34. J.G. Kirkwood, *Phys. Rev.* **44**, 31 (1933)
35. A. Boushehri et al., *J. Phy. Soc. Jpn* **69**, 6 (2000)
36. S.V. Churakov, M. Gottschalk, *Geochimica Cosmochimica Acta* **67**, 2397 (2003)
37. J. Jung, M.S. Jhon, H.R. Francis, *J. Chem Phys.* **102**, 1349 (1995)
38. R. Redmer, B. Holst, H. Juranek, N. Nettelmann, V. Schwartz, *J. Phys. A: Mathematical and General* **39**, 4479 (2006)
39. C.M. Abramo, C. Caccamo, G. Guinta, *Phys. Rev. A* **34**, 4 (1986)
40. L. Koei et al., *J. Phys.: Condens. Matter* **19**, 016206 (2007)
41. R.D. Mc Carty et al., *Selected Properties of Hydrogen, National Bureau of Standards Monograph* (Washington, DC: NBS, 1981), p. 168
42. Q. Wang et al., *Mol. Phys.* **89**, 1105 (1996)
43. *Air Liquide, Gas Encyclopedia* (Elsevier, 1976)